
NNC: Neural-Network Control of Dynamical Systems on Graphs

Thomas Asikis
Computational Social Science
ETH Zurich
Zurich, Switzerland
asikist@ethz.ch

Lucas Böttcher
Computational Medicine, UCLA, Los Angeles, USA
Institute for Theoretical Physics,
ETH Zurich, Zurich, Switzerland
lucasb@ucla.edu

Nino Antulov-Fantulin
Computational Social Science
ETH Zurich
Zurich, Switzerland
anino@ethz.ch

Abstract

We study the ability of neural networks to steer or control trajectories of dynamical systems on graphs. In particular, we introduce a neural-network control (NNC) framework, which represents dynamical systems by neural ordinary differential equations (neural ODEs), and find that NNC can learn control signals that drive networked dynamical systems into desired target states. To identify the influence of different target states on the NNC performance, we study two types of control: (i) microscopic control and (ii) macroscopic control. Microscopic control minimizes the L2 norm between the current and target state and macroscopic control minimizes the corresponding Wasserstein distance. We find that the proposed NNC framework produces low-energy control signals that are highly correlated with those of optimal control. Our results are robust for a wide range of graph structures and (non-)linear dynamical systems.

1 Introduction

The control of dynamical processes on networks [47, 46] is a challenging task with various applications in engineering, biology, and the social sciences [6, 61]. Mathematically, systems are “controllable” if they can be steered from any initial state $\mathbf{x}(t_0)$ to any desired state \mathbf{x}^* in finite time¹. Many real-world systems are difficult to control due to their intricate dynamics and structural properties, such as small-world effects [74], heavy-tail degree distributions [63, 5], community structure [29], and small diameters [23, 42]. Dynamical processes on networks are common tools to model a wide range of real-world phenomena including information-transfer and opinion dynamics [21, 11, 12, 34], epidemic spreading [13, 3, 10], synchronization [64, 78], and (financial) distress propagation [22]. Continuous-time dynamics on complex networks can be described by different frameworks including Chapman–Kolmogorov- [73], Fokker–Planck- [54], stochastic differential- [1], and ordinary-differential equations (ODEs) [16, 31, 7]. In this work, we focus on ODE formulations of dynamical processes on graphs since these are among the most common models of network dynamics [62].

¹ Note that some references use the term “reachable” for what we call “controllable” [4] or mean by “controllable” that it is possible to find some external input function that drives a dynamical system to the origin [14].

An analytical condition for the controllability of linear time-invariant (LTI) systems was derived by Kalman in the 1960s [36] and is known today as Kalman’s rank criterion. In 1969, Popov, Belevitch, and Hautus [33] introduced another controllability test for LTI systems that relies on an eigenvalue problem. In the 1970s, the study of graph-theoretic maximum matching problems, which focus on the identification of the minimum number of control nodes, inspired the formulation of a structural controllability condition [43]. More recently, different large-scale social, technical, and biological networks were analyzed from a network controllability perspective [47]. Later it has been shown that the minimum number of control nodes is not fully determined by the degree distribution of the underlying network [20]. Note that the problem of finding a minimum set of control (i.e., driver) nodes for general graphs is NP-hard [58]. Moreover, the structural controllability conditions of Ref. [47] imply that 80% of nodes have to be controlled in gene regulatory networks, contradicting corresponding empirical findings [55]. A specific challenge for the control of networked dynamical systems is that the controllability properties of a dynamical process defined on the edges of a network significantly differ from those of nodal dynamics [56]. The authors of Ref. [69] outlined that the structural problem of finding the minimal set of driver nodes has (sub)-modular properties. Their findings were later corrected and supplemented [59, 70]. Furthermore, Ref. [77] addresses the important issue of the amount of energy that is needed to control LTI systems and identifies scaling laws for the lower and upper energy bounds. To solve general non-linear optimal control problems, two main approaches are used: (i) Pontryagin’s maximum principle [49, 37, 51] and (ii) Bellman’s (approximate) dynamic programming [80, 25, 8, 71, 39].

In this paper, we propose a neural-network control (NNC) framework, that uses a neural-ODE representation of an underlying dynamical system with control signals on graphs (see Fig. 1). In Sec. 2, we provide an overview of concepts from dynamical systems and control theory and formulate conditions for the learnability of neural control functions. In Sec. 3, we introduce our neural-network control (NNC) framework. To validate the applicability of NNC, we apply it to different linear and non-linear dynamics in Sec. 4. Finally in Sec. 5, we discuss our results and conclude.

2 Dynamical Systems on Graphs and Control

A graph (i.e., network) $G(V, E)$ is an ordered pair, where V and $E \subseteq V \times V$ are the corresponding sets of $|V| = N$ nodes and edges. Throughout this paper, without loss of generality, we study dynamical systems on undirected networks with unweighted edges and an adjacency-matrix \mathcal{A} , which has non-zero elements \mathcal{A}_{ij} if and only if nodes i and j are connected.

We describe networked dynamical systems by ODEs of the form

$$\dot{\mathbf{x}}(t) = f(\mathbf{x}(t), \mathcal{A}, \mathbf{u}(t)), \quad (1)$$

where $\mathbf{x}(t) \in \mathbb{R}^N$ denotes the state vector and $\mathbf{u}(t) \in \mathbb{R}^M$ ($M \leq N$) an external control. We use Newton’s dot notation for differentiation $\dot{\mathbf{x}}(t)$, which is equivalent to Leibniz’s notation $\frac{d}{dt}\mathbf{x}(t)$. The function f in Eq. (1) accounts for both (time-dependent) interactions between nodes and the influence of external control signals on the evolution of $\mathbf{x}(t)$. In principle, Eq. (1) can be solved numerically, for instance using an explicit Euler scheme: For some given state $\mathbf{x}(t)$ at time t , the state of the system at time $t + \Delta t$ is $\mathbf{x}(t + \Delta t) = \mathbf{x}(t) + \Delta t f(\mathbf{x}(t), \mathbf{u}(t))$. Apart from an Euler forward integration scheme, there exist many more numerical methods [68] to solve Eq. (1). We use the expression $\text{ODESolve}(\mathbf{x}(t), t, T, f, \mathbf{u}(t))$ to indicate a generic ODE solver that uses the right-hand side of Eq. (1) as input and computes $\mathbf{x}(T)$ for a given $\mathbf{x}(t)$ if $T > t$. In Sec. 4, we employ Dormand–Prince, Adams–Bashford, and Runge–Kutta schemes as our ODESolve methods. One specific example of networked dynamical systems with a wide range of applications are binary-state dynamics on graphs

$$\dot{x}_i(t) = L(x_i(t)) + \sum_{j=1}^N \mathcal{A}_{i,j} Q(x_i(t), x_j(t)), \quad (2)$$

where $L(x_i(t))$ describes self-interactions and $Q(x_i(t), x_j(t))$ accounts for pair-wise interactions between neighbours. Note that we omit the control signal $\mathbf{u}(t)$ in Eq. (2) for notational simplicity. With appropriate choices of functions $L(\cdot)$ and $Q(\cdot)$, the ODE system Eq. (2) can model [7] epidemic processes, biochemical dynamics, birth–death processes, and regulatory dynamics. In this context, $x_i(t)$ represents the infectiousness level, reactant concentration, population, and gene expression level at node i .

Linear Time-Invariant Systems. For a broad range of systems such as (quantum) random walks [57, 18], search algorithms [60, 30], and social interactions [21, 11, 12, 34], it is possible to rewrite Eq. (1) in terms of networked linear time-invariant (LTI) systems $\dot{\mathbf{x}}(t) = A\mathbf{x}(t) + B\mathbf{u}(t)$ where $A \in \mathbb{R}^{N \times N}$ is a matrix that represents interactions between nodes (e.g., traffic/information flow and social ties) and $B \in \mathbb{R}^{N \times M}$ is a driver matrix that connects control signals with corresponding nodes. The outlined problem setting is known as the control problem of LTI systems [14].

Optimal Control. For LTI systems, it is possible to derive an optimal control (OC) [47] that minimizes the energy $\mathcal{E}[\mathbf{u}(t)] = \int_0^t \|\mathbf{u}(t)\|_2^2 dt$, where $\|\cdot\|_2$ denotes the L2 norm. For more details, see Sec. S1.1. Although analytical solutions of the outlined control problem exist for LTI systems [77], calculating numerical approximations of Eq. (S4) may involve numerical instabilities and can be computationally expensive for large systems. Numerical methods are also required for general non-linear ODE systems, which do not have analytic tractable solutions of optimal control signals.

One possibility to solve non-linear control problems is Pontryagin’s maximum principle [49, 37, 51], which is based on variational calculus and transforms the original infinite-dimensional control problem to a boundary-value problem in a Hamiltonian framework. The downside of this approach is that the resulting boundary-value problems are often very difficult to solve. An alternative to variational methods is provided by Bellman’s dynamic programming, which relies on the Hamilton–Jacobi–Bellman (HJB) equation. Given a quadratic loss on the control input, the HJB equation can be transformed into a partial-differential equation (PDE) [25]. Dynamic programming and Pontryagin’s maximum principle are connected through the viscosity solutions of the aforementioned PDEs [80]. However, in most cases, the HJB equation is hard to solve [8] and does not admit smooth solutions [26]. Most reinforcement-learning-based controls [71] rely on optimizing the HJB equation and can be viewed as an approximation of the dynamic programming [39] approach.

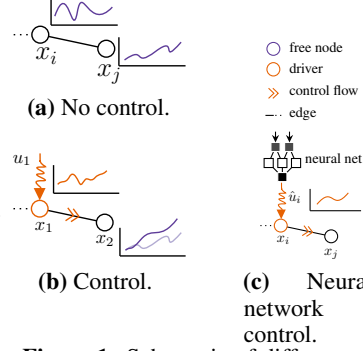


Figure 1: Schematic of different control approaches.

Driver node selection. Before controlling a certain system, we need to identify the set of driver nodes that are able to fully control the dynamics on a graph. Usually, we are interested in a problem of finding a minimum set of driver nodes, which is equivalent to the graph-theoretical problems of maximum matching or minimum edge dominating sets [19, 76]. However, for general graphs finding the maximum matching set is NP-hard [28, 58]. In our NNC framework, we determine driver nodes according to the maximum matching method described in Ref. [47]. We denote the set of driver nodes by $\mathbb{B} \subseteq V$, with cardinality M . The corresponding driver matrix is $B = \delta_{ij \in \mathbb{B}} \in \mathbb{R}^{N \times M}$, where δ_{ij} is the Kronecker delta.

Although literature is rich in studies on identifying driver node placement on graphs, there is considerably fewer work which addresses a way how to (efficiently) find control inputs for large-scale graph dynamics. The NNC framework that we propose can be used to control both linear and non-linear graph dynamical systems with different loss functions. Our approach is of particular relevance for control problems with unknown and intractable optimal control functions. It is based on universal approximation theorems for the approximation of continuous-time control functions with neural networks and learns control inputs directly from the dynamics. Finally, contrary to other optimal control approaches [77, 25, 49, 37, 51], we do not impose a control energy constraint directly on our optimization loss function, improving the learning efficiency.

3 Neural-Network Control

3.1 Learnability of Neural Control for LTI Systems

As reachability of a target state \mathbf{x}^* from an initial state $\mathbf{x}(t_0)$ implies the existence of a control function $\mathbf{u}(t)$, we now focus on the question whether $\mathbf{u}(t)$ can be learned (i.e., approximated) by a neural network.

Corollary 1. *Given that (i) a target state \mathbf{x}^* is reachable with continuous time dynamics $f(\mathbf{x}, \mathbf{u})$ (see Eq. (1)) and (ii) the control function $\mathbf{u}(t)$ is continuous or Lebesgue integrable in its domain, a neural network for which a corresponding universal approximation theorem applies can approximate a control function $\hat{\mathbf{u}}(t; \mathbf{w}) \rightarrow \mathbf{u}(t)$ by learning parameters \mathbf{w} .*

Corollary 2. In LTI systems, existence and learnability of a control function are guaranteed for any pair of initial and target states $(\mathbf{x}(t_0), \mathbf{x}^*)$ given that the Kalman-rank condition is satisfied.

In practice, Corollary 2 implies that control inputs for LTI systems should be learnable regardless of the choice of initial and target states. Furthermore, LTI systems are controllable for arbitrary time $T > 0$ [2], further reducing the choice of parameters for experimental evaluation. For more details on the learnability of control functions, see Sec. S1.2.

3.2 Neural ODE Control

As outlined in Corollary 1 and Refs. [15, 35, 79, 9], it is possible to use neural networks to learn an approximation $\hat{\mathbf{u}}$ of a control function \mathbf{u} . Neural ODEs [17] allow us to approximate a continuous time interaction and express the control function $\hat{\mathbf{u}}(t; \mathbf{w})$ as a parameterized neural network (see Fig. 2). For any neural-network architecture, we summarize our NNC approach in Algorithms 1 and 2.

Algorithm 1: A generic algorithm that describes the parameter learning of NNC.

```

Result:  $\mathbf{w}$ 
1 Init:  $\mathbf{x}_0, \mathbf{w}, f(\cdot), \text{ODESolve}(\cdot), J(\cdot), \mathbf{x}^*, \text{use\_adjoint}$ ;
2 Params:  $\eta, \text{epoch}$ ;
3  $\text{epoch} \leftarrow 0$ ;
4 while  $\text{epoch} < \text{epochs}$  do
5    $t \leftarrow 0$ ;
6    $\mathbf{x} \leftarrow \mathbf{x}_0$ ;
7   // Generate a trajectory based on NNC.
8    $\mathbf{x} \leftarrow \text{ODESolve}(\mathbf{x}, 0, T, f, \hat{\mathbf{u}}(\mathbf{x}, t; \mathbf{w}))$ ;
9   // Generic Quasi-Newton update
10   $\mathbf{w} \leftarrow \mathbf{w} - \eta \mathbf{H}^{-1} \nabla_{\mathbf{w}} J(\mathbf{x}, \mathbf{x}^*)$ 
11 end

```

Algorithm 2: A simple ODESolve implementation.

```

1 Function  $\text{ODESolve}(\mathbf{x}, t, T, f, \hat{\mathbf{u}}(\mathbf{x}, t; \mathbf{w}))$ :
2   // Euler Method
3   while  $t \leq T$  do
4     // Computational graph is
5     // preserved through time
6     // gradients flow through  $\mathbf{x}$ 
7      $\hat{\mathbf{u}} \leftarrow \hat{\mathbf{u}}(\mathbf{x}, t; \mathbf{w})$ ;
8      $\mathbf{x} \leftarrow \mathbf{x} + \tau f(\mathbf{x}, \hat{\mathbf{u}})$ ;
9     // Step  $\tau$  could be adapted
10     $t \leftarrow t + \tau(t)$ ;
11  end
12  return  $\mathbf{x}$ ;
13 end

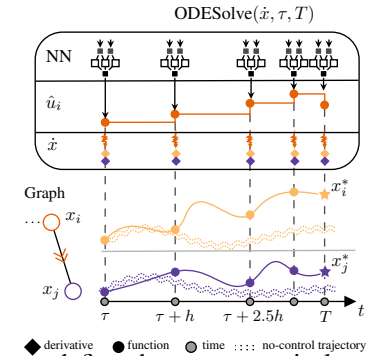
```

Below, we discuss the relationship between loss function and possible target states in terms of two types of loss functions: (i) microscopic loss and (ii) macroscopic loss.

Microscopic Loss. The aim of this type of control is to steer the state of each node towards the corresponding value of the target state vector \mathbf{x}^* at time t . It can be implemented by minimizing the differences between individual entries of the current and target state vector. One possible loss-function choice is the mean-square error $J(\mathbf{x}(t), \mathbf{x}^*) = \frac{1}{N} \|\mathbf{x}(t) - \mathbf{x}^*\|_2^2$. Microscopic control is a common tool in industrial applications and may be used to steer electric and mechanical systems [44]. Since there may exist several control trajectories $\mathbf{u}(t)$ that can reach the target state \mathbf{x}^* , the action cost (e.g., “energy”) might also be considered when selecting the optimal trajectory.

Macroscopic Loss. For the control of certain complex systems, it is more realistic to constrain the target state by a macroscopic property [66, 6] (e.g., the distributions of node states in the system). In order to characterize the loss with respect to a macroscopic target, we use a variant of the Wasserstein metric over empirical distributions [40]. For a sequence of ordered elements $x_1 \leq x_2 \leq \dots \leq x_N$ with $x_i \in \mathbb{R}$ and $y_1 \leq y_2 \leq \dots \leq y_N$ with $y_i \in \mathbb{R}$, we associate the corresponding empirical distributions $\alpha(x) = \frac{1}{N} \sum_i \delta(x - x_i)$, $\beta(y) = \frac{1}{N} \sum_i \delta(y - y_i)$, where $\delta(\cdot)$ denotes the Dirac delta function. For empirical distributions, the p-Wasserstein metric $W_p(\alpha, \beta)$ can be obtained via $W_p(\alpha, \beta)^p = \frac{1}{N} \sum_i |x_i - y_i|^p$, which is essentially the L^p norm of two vectors of the same size with ordered values. For a vector \mathbf{x} of node states, we denote the corresponding macroscopic property vector by $\tilde{\mathbf{x}}$. Its elements are sorted in an ascending way, i.e. $\tilde{x}_i \leq \tilde{x}_{i+1}$ ($1 \leq i \leq N - 1$). We can now define the macroscopic loss $J(\mathbf{x}(t), \tilde{\mathbf{x}}^*) = \frac{1}{N} \|\tilde{\mathbf{x}}(t) - \tilde{\mathbf{x}}^*\|_2^2$, which corresponds to the 2-Wasserstein metric [40] of two em-

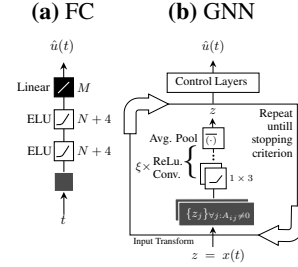
Figure 2: NNC: Control is learned within the ODESolver.



pirical distributions associated with the elements of state vector $\mathbf{x}(t)$ at time t and macroscopic target $\tilde{\mathbf{x}}^*$.

NNC architectures. Our experiments indicate that large numbers of non-smooth activations, large learning rates, and the absence of mechanisms to smooth loss functions, often lead to either stiff ODE trajectories or problems of neural networks to learn control inputs due to large losses. Designing an appropriate training routine and choosing appropriate activation functions is essential for high-performance NNCs. After hyper-parameter optimization, we designed two architectures for our experiments: (i) a time dependent fully connected control model $\hat{\mathbf{u}}(t)$ for LTI systems similar to optimal control and (ii) a Graph Convolutional NNC (class of Graph Neural Networks (GNNs) [75]) involving feedback control $\hat{\mathbf{u}}(\mathbf{x}(t))$ for non-linear dynamics. When using feedback control $\hat{\mathbf{u}}(\mathbf{x}(t))$ over a finite time horizon, the input state $\mathbf{x}(t)$ might reoccur. As a deterministic model, the neural network then requires the time variable t as input similar to generate a different control value². The Exponential Linear Unit (ELU) is used as an activation for the LTI case, as it provides a smooth alternative to the Rectified Linear Unit [72]. A large number of ReLU activations often leads to numerical instabilities during training, as the discontinuity of its derivative around 0 seems to make the ODE stiff and hence difficult to integrate with an ODE solver. For the control of LTI systems, we use the LBFGS optimizer, which is a quasi-newton optimizer that relies on the approximation of the inverse Hessian [45]. For non-linear systems, a non-parametrized version of the Adam optimizer is used [38].

Figure 3: Neural network architectures.



4 Experimental Setting and Performance

Although learnability is guaranteed for neural networks and control functions that satisfy Corollary 1, it may not be the case that NNC converges within reasonable time periods. To test the convergence and performance properties of the proposed NNC framework, we perform different numerical experiments on the following graphs with $N = 1024$ nodes: (i) square lattice with 512 driver nodes, (ii) random tree with 573 driver nodes, and (iii) Barabási–Albert graph with 714 driver nodes and attachment parameter $m = 1$. We evaluate the performance of the proposed neural network architectures for microscopic and macroscopic control tasks in terms of energy \mathcal{E} and loss function J values. In this section, we discuss the results for the square lattice, and in the SM we extend our analyses to other graph structures and experimental parameters.

To train NNC and account for dynamic interaction intervals, we use the Dormand–Prince [67] ODE solver [17] for all presented control cases. Performance evaluation is done on a fixed number of interactions to avoid performance artifacts from varying interaction intervals between different methods. For each control interaction³ the outlined NNC algorithm changes the control signal at a fixed time step $t = m\Delta t$, $m \in \{0, 1, 2, \dots\}$.

For performance evaluation and baseline comparisons in the LTI case, we employ a classical Runge–Kutta scheme that uses the interaction interval Δt as integration time step. In the non-linear case, we use the implicit Adams–Bashforth (multistep) method [50, 17] to determine and limit possible effects of stiffness-related instabilities. This method has varying time steps, but control interactions still happen at the predetermined interval. We optimize hyperparameters (e.g., number of epochs, network architectures etc.) interactively for each control task. One training epoch corresponds to one full control trajectory on which the neural network is trained.

While applying NNC to the outlined control tasks, we use an adaptive learning rate to counteract issues related to stiff ODEs and large losses. Furthermore, as NNC overfits, its performance increases on high interaction frequencies and deteriorates in low ones. This behavior is evaluated in the microscopic LTI control task, for which we train NNC for 304 epochs and evaluate its performance

² This problem is similar to state aliasing in reinforcement learning (RL) [53]. Another possible way to address this issue is to extend/augment the model inputs with a hidden state that allows the network to preserve an internal state over time, following the intuition behind RNNs [41] and Augmented Neural ODEs [24].

³ We refer to control signal changes as “interactions” and evaluate different control scenarios for different values of that parameter.

Table 1: Aggregate results (median and Interquartile Range (IQR)) over samples for a lattice graph, microscopic (Table 1a) and macroscopic (Table 1b) control with Neural-Network Control (NNC) and Optimal Control (OC) of CT-LTI dynamics. Highlighted values indicate higher performance for the given metric and interval values.

(a) Microscopic control

Δt	Method	Energy		MSE loss	
		Median	IQR	Median	IQR
10^{-2}	NNC	1.06×10^5	2.27×10^4	9.69×10^{-3}	5.17×10^{-3}
	OC	1.76×10^5	2.8×10^4	2×10^{-1}	5.97×10^{-2}
10^{-3}	NNC	1.68×10^5	1.5×10^4	1.23×10^{-3}	3.98×10^{-4}
	OC	1.7×10^5	2.69×10^4	2.06×10^{-3}	5.9×10^{-4}
10^{-4}	NNC	1.68×10^5	1.49×10^4	2.54×10^{-4}	1.55×10^{-4}
	OC	1.69×10^5	2.68×10^4	2.49×10^{-5}	6.87×10^{-6}

(b) Macroscopic control

Method	Energy		Wasserstein	
	Median	IQR	Median	IQR
NNC	8.71×10^2	2.11×10^2	3.07×10^{-4}	4.79×10^{-5}
OC-Perm	2.33×10^6	7.56×10^5	1.45×10^{-3}	7.41×10^{-4}
NNC-OC-Perm	9.75×10^2	2.24×10^2	2.32×10^{-4}	2.27×10^{-5}

for $\Delta t = 0.01$. Then we resume training for 720 epochs and continue with a performance evaluation for smaller time steps $\Delta t = 0.001, 0.0001$. In the macroscopic case, NNC is trained for 64 epochs and in the non-linear case the network is trained for 100 epochs. For all cases, a training epoch lasts a few minutes. The best performing model in terms of loss J is always preserved and evaluated. Our implemented architecture designs are summarized in Fig. 3. A fully connected (FC) architecture is used for LTI. This architecture has several millions of parameters and for memory efficiency we use the adjoint method [17]. However, for non-linear dynamics on graphs, a simple FC architecture was not suitable anymore, and we switched to more complex GNN architectures. A GNN architecture [65] with less than 100 parameters is used for non-linear control. For more details on NNC architectures, see the SM.

4.1 LTI Control Experiments

Microscopic Loss Experiments. For LTI systems $\dot{\mathbf{x}}(t) = \mathcal{A}\mathbf{x}(t) + B\mathbf{u}(t)$, we set the control time parameter to $T = 0.5$ and determine the driver matrix B according to the maximum matching method. Other values of T do not affect reachability and controllability, but may introduce scaling problems that can lead to numerical overflows and neuron saturation.

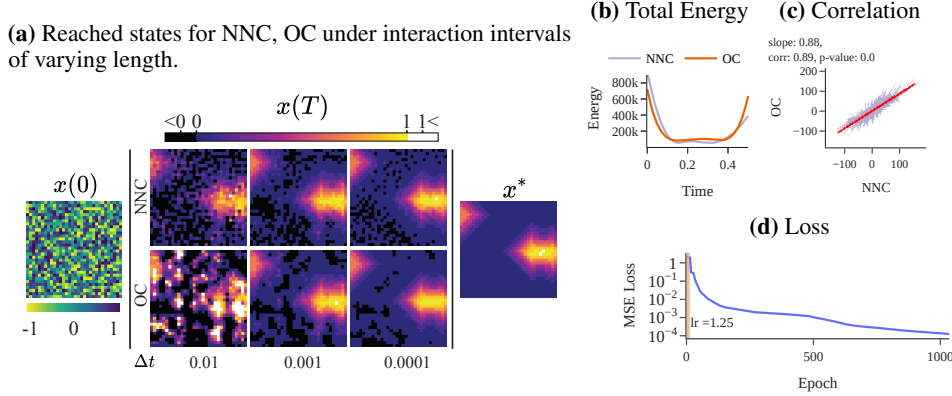
Higher interaction frequencies (i.e., larger numbers of control interactions) approximate continuous time systems with a higher precision, but lead to a considerable increase in computation time. For microscopic control of LTI systems, we evaluate each control scenario for $\Delta t \in \{10^{-2}, 10^{-3}, 10^{-4}\}$. For evaluation of other control cases we use $\Delta t = 10^{-3}$. This approach allows us to study the NNC performance for different interaction frequencies. As a baseline for LTI control, we use the optimal control (OC) framework of Ref. [47] (see Sec. S1.1 for further details). Optimal control is a continuous method and not affected by the step interval. For the approximation of the integral term in the Gramian calculation (see Eq. (S5)), we decompose the domain in 100 subintervals and apply Simpson’s quadrature.

For microscopic control, NNC shows superior performance for higher interaction intervals ($\Delta t = 10^{-2}, \Delta t = 10^{-3}$) in all evaluation metrics (see Table 1a). The performance superiority is evident especially when the control is discretized with $\Delta t = 10^{-2}$, which can be qualitatively confirmed by Fig. 4a. For the lowest interaction interval ($\Delta t = 10^{-4}$), optimal control outperforms NNC in terms of smaller loss values $J(\mathbf{x}(t), \mathbf{x}^*)$ and the energy difference between both types of control is within approximation error. The superior performance of optimal control in the limit $\Delta \rightarrow 0$ is expected from optimal control theory. Neural-network-control learning is stable once an appropriate learning-rate value is selected and numerical instabilities become less common (see Fig. 4d). A large number of training epochs and allowing the integrator to evaluate smaller interaction intervals could potentially further increase the neural network performance on lower interaction intervals.

An unexpected observation is the similarity of OC and NNC in terms of their energies $\mathcal{E}[\mathbf{u}(T)]$. Although we do not use any explicit energy regularization for training NNC, it achieves relatively low energy values Fig. 4b, which almost perfectly coincide with those of OC. We show the corresponding

correlations between the energy of NNC and OC in Fig. 4c. This behavior can be observed for different target states and graph structures (see Sec. S1.6 for a more detailed analysis). It is remarkable since NNC has a linear output activation (see Fig. 3a) and is still able to learn control inputs which are highly-correlated with those of OC.

Figure 4: Comparison of NNC and OC controls on a single microscopic control sample. Results are similar for other samples. (a) Controlling LTI system from random initial state to target state x^* with different number of control interactions Δt . NNC control shows stable performance across different time-scales. (b) NNC is having low energy control signal. (c) NNC and OC signals are highly correlated. (d) Stable training loss of NNC.



Macroscopic Loss Experiments. In Table 1b, we summarize the quantitative results on LTI macroscopic control with Wasserstein loss. We sample pairs $\{(\mathbf{x}_{0,i}, \mathbf{x}_i^*)\}_{i=1}^{100}$, where values for $\mathbf{x}_0, \mathbf{x}^*$ are i.i.d. samples from uniform and normal distributions, respectively. In order to use optimal control as a baseline with macroscopic constraint \mathbf{x}^* , we study the “OC-Perm” baseline, which is based on m random permutations $\{\mathbf{x}_i^*\}_{i=1}^m$ for each \mathbf{x}^* target constraint vector. Note that every sample $\{\mathbf{x}_i^*\}_{i=1}^m$ preserves the macroscopic constraint of the empirical distribution $\alpha(x) = \frac{1}{N} \sum_i \delta(x - x_i)$ associated with target state $\tilde{\mathbf{x}}^*$. In our experiments, we use $m = 1000$ random permutations in the OC-Perm baseline for each macroscopic target constraint. In doing so, we explore the ensemble $\{\mathbf{x}_i^*\}_{i=1}^m$ of possible microscopic targets that are all obeying the macroscopic property constraint $\tilde{\mathbf{x}}^*$. As expected, the OC-Perm baseline reaches the state, that has low Wasserstein distance from target state (2nd row of Table 1b). At the same time, the OC-Perm baseline takes large energy costs compared to our NNC approach (1st column of Table 1b). None of the $m = 1000$ evaluated permutations with OC-Perm managed to reach similar energy levels of NNC, indicating the difficulty of minimizing the energy with macroscopic constraint. To give more insights in the macroscopic loss constraint, we study an additional hybrid “NNC-OC-Perm” baseline. For the NNC-OC-Perm baseline, each target constraint $\tilde{\mathbf{x}}^*$ runs in two stages: (i) NNC control of $\mathbf{x}_0 \xrightarrow{\text{NNC}(\tilde{\mathbf{x}}^*)} \mathbf{x}_T$, which satisfies $\tilde{\mathbf{x}}^*$, and (ii) OC of $\mathbf{x}_0 \xrightarrow{\text{OC}(\mathbf{x}_T)} \hat{\mathbf{x}}_T$. We observe that both NNC and NNC-OC-Perm carry the initial state distribution to the target distribution in a similar manner (see Fig. S1a). The presented sample score is shown in Fig. S1e. For all samples, the minimum significant correlation value is 0.64 and only 4 samples score below 0.8.

4.2 Control of Non-Linear Dynamics

For the control of a non-linear dynamical system, we focus on a class of epidemic models (SIR-X) that accounts for quarantine interventions [48]. We extend the model [48], with dynamic control signals with graph topology. The dynamics of node i is described by a set of rate equations:

$$\begin{aligned}
 \dot{S}_i(t) &= -\beta S_i(t) \sum_j \mathcal{A}_{i,j} I_j(t) - (\kappa_{0,i} + \hat{u}_i(t) \mathbb{1}_{i \in \mathbb{B}}) S_i(t) \\
 \dot{I}_i(t) &= \beta S_i(t) \sum_j \mathcal{A}_{i,j} I_j(t) - \gamma I_i(t) - (\kappa_{0,i} + \hat{u}_i(t) \mathbb{1}_{i \in \mathbb{B}}) I_i(t) \\
 \dot{R}_i(t) &= \gamma I_i(t) + (\kappa_{0,i} + \hat{u}_i(t) \mathbb{1}_{i \in \mathbb{B}}) S_i(t), \\
 \dot{X}_i(t) &= (\kappa_{0,i} + \hat{u}_i(t) \mathbb{1}_{i \in \mathbb{B}}) I_i(t),
 \end{aligned} \tag{3}$$

subject to $\sum_i [S_i + I_i + R_i + X_i] = 1$ (i.e., the total population is conserved) and $\sum_i [\kappa_{0,i} + \hat{u}_i(t) \mathbb{1}_{i \in \mathbb{B}}] \leq K$ (i.e., the control budget is limited), where $I_i(t)$, $S_i(t)$, $R_i(t)$, and $X_i(t)$ denote the probability of node i to be infected, susceptible, recovered, and contained, respectively. The parameters β and γ are the infection and recovery rate, parameter $\kappa_{0,i}$ describes the effect of containment interventions (e.g., social/physical distancing) and the control signal $\hat{u}_i(t)$ is applied to driver nodes only and represents dynamic containment measures. The indicator function $\mathbb{1}_{i \in \mathbb{B}}$ has nonzero value 1 iff node i is a driver node. To determine the target time T , we observe the process without control and set its value to t , such that the mean infection over all nodes at time t is approximately zero $\bar{I}_i(t) \approx 0$. The SIR-X dynamics experiment ($\beta = 6, \gamma = 1.8, R_0 \approx 3.33$) is evolving on a square lattice, where the initial infection starts from a deterministic selection of nodes in the upper right quadrant. Our control goal is to constrain epidemic outbreaks (i.e., “flattening” the infection curve) in the subgraph G^* , which is located in the bottom-left quadrant (see Fig. 6). This goal can be formulated as the L2 microscopic loss w.r.t. the maximum point of an infection curve (see Sec. S1.7 for further details).

In order to select an appropriate baseline model, we briefly summarize some constraints that become relevant for the control of networked non-linear dynamics. Note that NNC has no direct information on which nodes are part of subgraph G^* , as it is only given via the loss-function value. A baseline that takes structural node properties (e.g., node degree) into the account, may be a good baseline for structural-heterogeneous graphs, but not for regular structures like lattices. Clearly, a weak baseline (RND) would be assigning random control inputs to driver nodes. However, a targeted constant control baseline (TCC), which in the presence of an “oracle” assigns constant control inputs to every driver node in G^* , is a strong baseline for constant control. In Fig. 5, we observe that NNC is providing strong protection with total energy costs that are not as high as TCC (see Table 2. We also studied the performance of dynamic control baselines, such as continuous-action RL, with fully connected neural networks or our variant (see Fig. 3b) as policy architecture and the training routines of SAC [32], TD3 [27], and A2C [52]. However, even after testing different reward designs and parameters settings, none managed to perform better than our baselines. It may be possible that extensive reward engineering, and other model upgrades may lead to better performance. More details are presented in Sec. S1.7 and S1.8.

Table 2: Energy and peak infection evaluation.

Control	$\max_t (\bar{I}(t))$	$E(T)$
TCC	0.068	14059.7
NNC	0.078	8354.7
RND	0.210	4687.0
F	0.430	0.0

Figure 5: SIRX control evaluation.

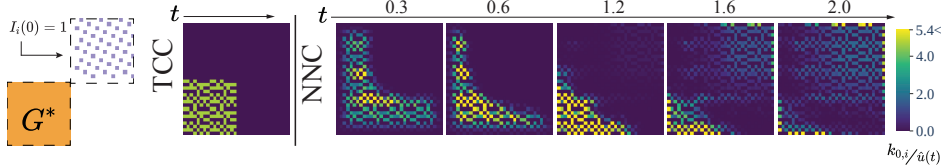
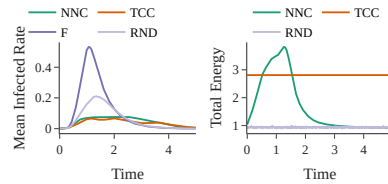


Figure 6: Initial infection, target subgraph, and control trajectories for SIR-X dynamics. Baselines: Targeted Constant Control (TCC), Random Constant Control (RND), and free dynamics with no control (F). Colorscale plots, represents 99.5% of the presented values for dynamics with NNC controls.

5 Discussion and Conclusion

Contrary to Ref. [17] that parameterizes the derivative of hidden states using neural networks, our neural-ODE systems describes controlled (non-)linear dynamics on graphs. Neural-network control approximates dynamical systems based on observations of the system-state evolution and determines control inputs according to pre-defined target states. In general, neural networks are able to approximate any control input as long as they satisfy corresponding universal approximation theorems. However, in practice, NNC needs to deal with different numerical hurdles such as large losses and stiffness problems of the underlying ODE systems. By testing NNC on various graph structures and dynamical systems, we provide evidence that these hurdles can be overcome with appropriate choices of both hyperparameters and numerical ODE solvers. Our results show that the control inputs of NNC

are highly-correlated with those of optimal control (OC), suggesting that NCC is having implicit energy regularization, resulting from the joint interplay of neural-network initialization, gradient descent, and ODE solvers. Future studies may further investigate this observation and study the effectiveness of NNC under additional constraints such as partial observability and delayed/noisy controls.

6 Broader Impact

Scientific advancements have been carried by the ability to quantify, predict, and finally control different phenomena and systems. Controlling dynamical systems has a wide range of application in many fields, ranging from engineering, finance, complexity science to social sciences and biology. In engineering, a lot of optimal and feedback control methods exist. However, our method may become useful for controlling large scale non-linear systems. For other fields, our method can be used to simulate and experimentally evaluate controlled continuous dynamics models. To provide evidence for the general applicability of our neural-network control (NNC) method, we apply it to a non-linear ODE system that describes networked epidemic processes. Researchers from other fields (e.g., biology) can use our method to generate meaningful controls on simulations that involve mass-action kinetics for proteins and gene regulatory dynamics, as long as a meaningful target and control can be defined.

In the field of computational social science, the proposed methods can be used to study the effects of certain control strategies on real-world phenomena such as the spread of disinformation (or “fake news campaigns”) on social media platforms. Current developments in deep learning have provided us with many useful tools that are used to simulate, analyze, and predict a wide spectrum of social dynamics. Still, the amount, granularity, and quality of data required to perform such studies often conflict with privacy, fair treatment, and autonomy of individuals. When designing experiments that involve any deep learning method, and especially NNC, privacy preservation and autonomy should be of the highest priority. For example, in our simulations, the selection of driver nodes is done without constraints. This should not be the case in a corresponding real-world application, especially in social systems where nodes are usually matched to individuals.

Frameworks of participatory and self-determined control should be developed in case of social studies, where individuals are free to choose whether they want to be selected as driver nodes. In such studies, individuals should be aware and consenting with a control scheme and its targets; otherwise, the ethics and motives behind such a study are highly questionable. Disruption of oppressive control strategies (e.g., propaganda and censorship) can be also quantitatively studied, as disrupting controls can be learned via NNC on continuous dynamics that describe those strategies. Studies on asymmetric control strategies, where competitive controls have highly varying budget constraints, can now be trained and studied with less implementation effort. Using a simulation-trained NNC to control real-world social systems directly may not produce expected results, as reality is not fully captured by ODE-type systems. All in all, NNC as all technological advancements should comply with the interests of a whole society and not to suppress individual freedoms.

Finally, we believe, that our work in machine learning and systems control will inspire and open novel theoretical and practical innovations in the fields of complex systems, computational social science, quantitative biology, and finance.

7 Acknowledgements

L.B. acknowledges financial support from the SNF Early Postdoc Mobility fellowship on “Multispecies interacting stochastic systems in biology”. N.A.-F. has been funded by the European Program scheme 'INFRAIA-01- 2018-2019: Research and Innovation action', grant agreement #871042 'SoBigData++: European Integrated Infrastructure for Social Mining and Big Data Analytics'. T.A. received financial support from the LCM – K2 Center within the framework of the Austrian COMET-K2 program.

References

- [1] ANDERSSON, H., AND BRITTON, T. *Stochastic epidemic models and their statistical analysis*, vol. 151. Springer Science & Business Media, 2012.
- [2] ANTSAKLIS, P. J., AND MICHEL, A. N. *A linear systems primer*. Springer Science & Business Media, 2007.
- [3] ANTULOV-FANTULIN, N., LANČIĆ, A., ŠMUC, T., ŠTEFANČIĆ, H., AND ŠIKIĆ, M. Identification of patient zero in static and temporal networks: Robustness and limitations. *Physical review letters* 114, 24 (2015), 248701.
- [4] ÅSTRÖM, K. J., AND MURRAY, R. M. *Feedback systems: an introduction for scientists and engineers*. Princeton University Press, 2010.
- [5] BARABÁSI, A.-L., AND ALBERT, R. Emergence of scaling in random networks. *science* 286, 5439 (1999), 509–512.
- [6] BARRAT, A., BARTHELEMY, M., AND VESPIGNANI, A. *Dynamical processes on complex networks*. Cambridge university press, 2008.
- [7] BARZEL, B., AND BARABÁSI, A.-L. Universality in network dynamics. *Nature physics* 9, 10 (2013), 673–681.
- [8] BELLMAN, R. E., AND DREYFUS, S. E. *Applied dynamic programming*. Princeton university press, 2015.
- [9] BHASIN, S., KAMALAPURKAR, R., JOHNSON, M., VAMVOUDAKIS, K. G., LEWIS, F. L., AND DIXON, W. E. A novel actor–critic–identifier architecture for approximate optimal control of uncertain nonlinear systems. *Automatica* 49, 1 (2013), 82–92.
- [10] BÖTTCHER, L., ANDRADE, J., AND HERRMANN, H. J. Targeted recovery as an effective strategy against epidemic spreading. *Scientific reports* 7, 1 (2017), 1–7.
- [11] BÖTTCHER, L., HERRMANN, H. J., AND GERSBACH, H. Clout, activists and budget: The road to presidency. *PloS one* 13, 3 (2018).
- [12] BÖTTCHER, L., MONTEALEGRE, P., GOLES, E., AND GERSBACH, H. Competing activists—political polarization. *Physica A: Statistical Mechanics and its Applications* 545 (2020), 123713.
- [13] BROCKMANN, D., AND HELBING, D. The hidden geometry of complex, network-driven contagion phenomena. *science* 342, 6164 (2013), 1337–1342.
- [14] BROGAN, W. L. *Modern Control Theory (3rd Ed.)*. Prentice-Hall, Inc., USA, 1991.
- [15] BUCCI, M. A., SEMERARO, O., ALLAUZEN, A., WISNIEWSKI, G., CORDIER, L., AND MATHELIN, L. Control of chaotic systems by deep reinforcement learning. *Proceedings of the Royal Society A* 475, 2231 (2019), 20190351.
- [16] CASTELLANO, C., AND PASTOR-SATORRAS, R. Thresholds for epidemic spreading in networks. *Physical review letters* 105, 21 (2010), 218701.
- [17] CHEN, R. T. Q., RUBANOVA, Y., BETTENCOURT, J., AND DUVENAUD, D. Neural ordinary differential equations. *Advances in Neural Information Processing Systems* (2018).
- [18] CHILDS, A. M. Universal computation by quantum walk. *Physical Review Letters* 102, 18 (2009), 180501.
- [19] COMMAULT, C., DION, J.-M., AND VAN DER WOUDE, J. W. Characterization of generic properties of linear structured systems for efficient computations. *Kybernetika* 38, 5 (2002), 503–520.
- [20] COWAN, N. J., CHASTAIN, E. J., VILHENA, D. A., FREUDENBERG, J. S., AND BERGSTROM, C. T. Nodal dynamics, not degree distributions, determine the structural controllability of complex networks. *PloS one* 7, 6 (2012).
- [21] DEGROOT, M. H. Reaching a consensus. *Journal of the American Statistical Association* 69, 345 (1974), 118–121.
- [22] DELPINI, D., BATTISTON, S., RICCABONI, M., GABBI, G., PAMMOLLI, F., AND CALDARELLI, G. Evolution of controllability in interbank networks. *Scientific Reports* 3, 1 (Apr. 2013).

- [23] DOROGOVTSSEV, S. N., GOLTSEV, A. V., AND MENDES, J. F. Critical phenomena in complex networks. *Reviews of Modern Physics* 80, 4 (2008), 1275.
- [24] DUPONT, E., DOUCET, A., AND TEH, Y. W. Augmented neural odes. In *Advances in Neural Information Processing Systems* (2019), pp. 3134–3144.
- [25] FLEMING, W. H., AND SONER, H. M. *Controlled Markov processes and viscosity solutions*, vol. 25. Springer Science & Business Media, 2006.
- [26] FRANKOWSKA, H. Nonsmooth solutions of hamilton-jacobi-bellman equation. In *Modeling and Control of Systems*. Springer-Verlag, 1989, pp. 131–147.
- [27] FUJIMOTO, S., HOOF, H., AND MEGER, D. Addressing function approximation error in actor-critic methods. In *International Conference on Machine Learning* (2018), pp. 1587–1596.
- [28] GAREY, M. R., AND JOHNSON, D. S. *Computers and intractability*, vol. 174. freeman San Francisco, 1979.
- [29] GIRVAN, M., AND NEWMAN, M. E. Community structure in social and biological networks. *Proceedings of the national academy of sciences* 99, 12 (2002), 7821–7826.
- [30] GKANTSIDIS, C., MIHAIL, M., AND SABERI, A. Random walks in peer-to-peer networks. In *IEEE INFOCOM 2004* (2004), vol. 1, IEEE.
- [31] GLEESON, J. P. Binary-state dynamics on complex networks: Pair approximation and beyond. *Physical Review X* 3, 2 (2013), 021004.
- [32] HAARNOJA, T., ZHOU, A., ABBEEL, P., AND LEVINE, S. Soft actor-critic: Off-policy maximum entropy deep reinforcement learning with a stochastic actor. In *International Conference on Machine Learning* (2018), pp. 1861–1870.
- [33] HAUTUS, M. L. Controllability and observability conditions of linear autonomous systems. In *Indagationes Mathematicae (Proceedings)* (1969), vol. 72, pp. 443–448.
- [34] HOFERER, M., BÖTTCHER, L., HERRMANN, H. J., AND GERSBACH, H. The impact of technologies in political campaigns. *Physica A: Statistical Mechanics and its Applications* 538 (2020), 122795.
- [35] HUA, C., AND GUAN, X. Adaptive control for chaotic systems. *Chaos, Solitons & Fractals* 22, 1 (2004), 55–60.
- [36] KALMAN, R. E., ET AL. Contributions to the theory of optimal control. *Bol. soc. mat. mexicana* 5, 2 (1960), 102–119.
- [37] KAMIEN, M. I., AND SCHWARTZ, N. L. Sufficient conditions in optimal control theory. *Journal of Economic Theory* 3, 2 (1971), 207–214.
- [38] KINGMA, D. P., AND BA, J. Adam: A method for stochastic optimization. *arXiv preprint arXiv:1412.6980* (2014).
- [39] KIUMARSI, B., VAMVOUDAKIS, K. G., MODARES, H., AND LEWIS, F. L. Optimal and autonomous control using reinforcement learning: A survey. *IEEE transactions on neural networks and learning systems* 29, 6 (2017), 2042–2062.
- [40] KOLOURI, S., NADJABI, K., SIMSEKLI, U., BADEAU, R., AND ROHDE, G. Generalized sliced wasserstein distances. In *Advances in Neural Information Processing Systems* (2019), pp. 261–272.
- [41] KOUTNIK, J., GREFF, K., GOMEZ, F., AND SCHMIDHUBER, J. A clockwork rnn. In *International Conference on Machine Learning* (2014), pp. 1863–1871.
- [42] LESKOVEC, J., CHAKRABARTI, D., KLEINBERG, J., FALOUTSOS, C., AND GHAHRAMANI, Z. Kronecker graphs: An approach to modeling networks. *Journal of Machine Learning Research* 11, Feb (2010), 985–1042.
- [43] LIN, C.-T. Structural controllability. *IEEE Transactions on Automatic Control* 19, 3 (1974), 201–208.
- [44] LIPTAK, B. G. *Instrument Engineers’ Handbook, Volume Two: Process Control and Optimization*. CRC press, 2018.
- [45] LIU, D. C., AND NOCEDAL, J. On the limited memory bfgs method for large scale optimization. *Mathematical programming* 45, 1-3 (1989), 503–528.

- [46] LIU, Y.-Y., AND BARABÁSI, A.-L. Control principles of complex systems. *Reviews of Modern Physics* 88, 3 (2016), 035006.
- [47] LIU, Y.-Y., SLOTINE, J.-J., AND BARABÁSI, A.-L. Controllability of complex networks. *nature* 473, 7346 (2011), 167–173.
- [48] MAIER, B. F., AND BROCKMANN, D. Effective containment explains subexponential growth in recent confirmed covid-19 cases in china. *Science* 368, 6492 (2020), 742–746.
- [49] MANGASARIAN, O. L. Sufficient conditions for the optimal control of nonlinear systems. *SIAM Journal on control* 4, 1 (1966), 139–152.
- [50] MARCINIAK, A., AND JANKOWSKA, M. A. Interval methods of adams-bashforth type with variable step sizes. *Numerical Algorithms* (2019), 1–28.
- [51] MCSHANE, E. The calculus of variations from the beginning through optimal control theory. *SIAM journal on control and optimization* 27, 5 (1989), 916–939.
- [52] MNIH, V., BADIA, A. P., MIRZA, M., GRAVES, A., LILICRAP, T., HARLEY, T., SILVER, D., AND KAVUKCUOGLU, K. Asynchronous methods for deep reinforcement learning. In *International conference on machine learning* (2016), pp. 1928–1937.
- [53] MNIH, V., KAVUKCUOGLU, K., SILVER, D., GRAVES, A., ANTONOGLU, I., WIERSTRA, D., AND RIEDMILLER, M. Playing atari with deep reinforcement learning. *arXiv preprint arXiv:1312.5602* (2013).
- [54] MOYAL, J. E. Stochastic processes and statistical physics. *Journal of the Royal Statistical Society. Series B (Methodological)* 11, 2 (1949), 150–210.
- [55] MÜLLER, F.-J., AND SCHUPPERT, A. Few inputs can reprogram biological networks. *Nature* 478, 7369 (Oct. 2011), E4–E4.
- [56] NEPUSZ, T., AND VICSEK, T. Controlling edge dynamics in complex networks. *Nature Physics* 8, 7 (2012), 568–573.
- [57] NOH, J. D., AND RIEGER, H. Random walks on complex networks. *Physical review letters* 92, 11 (2004), 118701.
- [58] OLSHEVSKY, A. Minimal controllability problems. *IEEE Transactions on Control of Network Systems* 1, 3 (2014), 249–258.
- [59] OLSHEVSKY, A. On (non)supermodularity of average control energy. *IEEE Transactions on Control of Network Systems* 5, 3 (2018), 1177–1181.
- [60] PAGE, L., BRIN, S., MOTWANI, R., AND WINOGRAD, T. The pagerank citation ranking: Bringing order to the web. Tech. rep., Stanford InfoLab, 1999.
- [61] PASTOR-SATORRAS, R., CASTELLANO, C., VAN MIEGHEM, P., AND VESPIGNANI, A. Epidemic processes in complex networks. *Rev. Mod. Phys.* 87 (Aug 2015), 925–979.
- [62] PORTER, M. A., AND GLEESON, J. P. Dynamical systems on networks. *Frontiers in Applied Dynamical Systems: Reviews and Tutorials* 4 (2016).
- [63] PRICE, D. J. D. S. Networks of scientific papers. *Science* (1965), 510–515.
- [64] RODRIGUES, F. A., PERON, T. K. D., JI, P., AND KURTHS, J. The kuramoto model in complex networks. *Physics Reports* 610 (2016), 1–98.
- [65] SCARSELLI, F., GORI, M., TSOI, A. C., HAGENBUCHNER, M., AND MONFARDINI, G. The graph neural network model. *IEEE Transactions on Neural Networks* 20, 1 (2008), 61–80.
- [66] SETHNA, J., ET AL. *Statistical mechanics: entropy, order parameters, and complexity*, vol. 14. Oxford University Press, 2006.
- [67] SHAMPINE, L. F. Some practical runge-kutta formulas. *Mathematics of computation* 46, 173 (1986), 135–150.
- [68] SHAMPINE, L. F. *Numerical solution of ordinary differential equations*. Routledge, 2018.
- [69] SUMMERS, T. H., CORTESI, F. L., AND LYGEROS, J. On submodularity and controllability in complex dynamical networks. *IEEE Transactions on Control of Network Systems* 3, 1 (2015), 91–101.

- [70] SUMMERS, T. H., CORTESI, F. L., AND LYGEROS, J. Corrections to “on submodularity and controllability in complex dynamical networks”. *IEEE Transactions on Control of Network Systems* 5, 3 (2018), 1503–1503.
- [71] SUTTON, R. S., AND BARTO, A. G. *Reinforcement learning: An introduction*. MIT press, 2018.
- [72] TROTTIER, L., GIGU, P., CHAIB-DRAA, B., ET AL. Parametric exponential linear unit for deep convolutional neural networks. In *2017 16th IEEE International Conference on Machine Learning and Applications (ICMLA)* (2017), IEEE, pp. 207–214.
- [73] VAN KAMPEN, N. G. *Stochastic processes in physics and chemistry*, vol. 1. Elsevier, 1992.
- [74] WATTS, D. J., AND STROGATZ, S. H. Collective dynamics of ‘small-world’ networks. *nature* 393, 6684 (1998), 440.
- [75] XU, K., HU, W., LESKOVEC, J., AND JEGELKA, S. How powerful are graph neural networks? *arXiv preprint arXiv:1810.00826* (2018).
- [76] YAMADA, T., AND FOULDS, L. R. A graph-theoretic approach to investigate structural and qualitative properties of systems: A survey. *Networks* 20, 4 (1990), 427–452.
- [77] YAN, G., REN, J., LAI, Y.-C., LAI, C.-H., AND LI, B. Controlling complex networks: How much energy is needed? *Physical review letters* 108, 21 (2012), 218703.
- [78] YEUNG, M. S., AND STROGATZ, S. H. Time delay in the kuramoto model of coupled oscillators. *Physical Review Letters* 82, 3 (1999), 648.
- [79] YOO, S. J., PARK, J. B., AND CHOI, Y. H. Stable predictive control of chaotic systems using self-recurrent wavelet neural network. *international journal of control, automation, and systems* 3, 1 (2005), 43–55.
- [80] ZHOU, X. Maximum principle, dynamic programming, and their connection in deterministic control. *Journal of Optimization Theory and Applications* 65, 2 (1990), 363–373.

S1 Supplementary Material for NNC: Neural-Network Control of Dynamical Systems on Graphs

S1.1 Linear Time-Invariant Systems

Mathematically, networked linear time-invariant (LTI) systems are described by

$$\dot{\mathbf{x}}(t) = A\mathbf{x}(t) + B\mathbf{u}(t) \quad (\text{S1})$$

where $A \in \mathbb{R}^{N \times N}$ is a matrix that represents interactions between nodes (e.g., traffic/information flow and social ties) and $B \in \mathbb{R}^{N \times M}$ is a driver matrix that connects control signals with corresponding nodes. The outlined problem setting is known as the control problem of LTI systems [2]. As for the more general dynamical system Eq. (1), we will approximate external inputs $B\mathbf{u}(t)$ with a family of parameterized neural networks and refer to this type of control problem as NNC of LTI systems on graphs.

An LTI system is controllable if and only if

$$C = [B, AB, A^2B, \dots, A^{N-1}B] \quad (\text{S2})$$

has full rank, which is known as Kalman's rank condition [6]. Intuitively, this condition is a consequence of analyzing products of the Taylor expansion elements of the matrix exponential $\exp[A(t - \tau)]$, which appears in the solution $\mathbf{x}(t) = \int_0^t \exp[A(t - \tau)]B\mathbf{u}(\tau) d\tau$ with $\mathbf{x}(0) = \mathbf{0}$, and matrix B . For LTI systems, there exist optimal control methods [8] that minimize the energy

$$\mathcal{E}[\mathbf{u}(t)] = \int_0^T \|\mathbf{u}(t)\|_2^2 dt, \quad (\text{S3})$$

where $\|\cdot\|_2$ denotes the L2 norm. The corresponding optimal control signal is

$$\mathbf{u}(t) = B^\top e^{A(T-t)} W(T)^{-1} \mathbf{v}(T), \quad (\text{S4})$$

where $\mathbf{v}(T) = \mathbf{x}(T) - e^{AT} \mathbf{x}_0$ is the difference between target state $\mathbf{x}(T)$ and initial state $\mathbf{x}(0)$ under free evolution. The matrix $W(T)$ is the controllability Gramian and defined as:

$$W(T) = \int_0^T e^{At} B B^\top e^{A^\top t} dt. \quad (\text{S5})$$

The external input $\mathbf{u}(t)$ of Eq. (S4) is chosen such that the applied control minimizes energy and is solved by Pontryagin's maximum principle [18].

S1.2 Learnability of Neural Control for LTI Systems

As reachability of a target state \mathbf{x}^* from an initial state $\mathbf{x}(t_0)$ implies the existence of a control function $\mathbf{u}(t)$ [9], we now focus on the question whether $\mathbf{u}(t)$ can be learned (i.e., approximated) by a neural network.

There exist several common formulations of universal approximation theorems (see e.g. the Stone–Weierstrass theorem [13]), yet in this paper we focus on a subset of theorems relevant to neural-network architectures [19, 11, 12, 5]. Single-layer neural networks with arbitrary numbers of ridge-activation-function neurons can approximate any continuous function $g : \mathbb{R}^N \rightarrow \mathbb{R}$ [7]. The universal-approximation capability of single-layer neural networks also extends to arbitrary-depth convolutional and recurrent-neural networks [19, 11, 12]. Multilayer neural networks with N inputs and bounded numbers $K \leq N + 4$ of ReLU-activation-function neurons per layer can approximate Lebesgue-integrable functions [5]. Approximations for a single output can be extended to M outputs by using M neural networks that satisfy universal approximation. The proposed framework and its ability to address a wide range of control challenges is motivated by the following corollary that extends the universal approximation theorems of Refs. [19, 11, 12, 5].

Corollary 1. *Given that (i) a target state \mathbf{x}^* is reachable with continuous time dynamics $f(\mathbf{x}, \mathbf{u})$ (see Eq. (1)) and (ii) the control function $\mathbf{u}(t)$ is continuous or Lebesgue integrable in its domain, a neural network for which a corresponding universal approximation theorem applies can approximate a control function $\hat{\mathbf{u}}(t; \mathbf{w}) \rightarrow \mathbf{u}(t)$, by learning parameters \mathbf{w} .*

Proof. Reachability of a target state guarantees the existence of a control function u [9]. A continuous or Lebesgue-integrable control function can be approximated via a neural network architecture that satisfies a corresponding universal approximation theorem [19, 11, 12, 5]. \square

Corollary 1 can be also extended to LTI systems.

Corollary 2. *In LTI systems, existence and learnability of a control function are guaranteed for any pair of initial and target states $(\mathbf{x}(t_0), \mathbf{x}^*)$ given that the Kalman-rank condition is satisfied.*

Proof. If an LTI system satisfies the Kalman-rank condition, it is controllable for any pair of initial and target states $(\mathbf{x}(t_0), \mathbf{x}^* \in X)$ [1]. The control function is continuous and can therefore be approximated by neural networks that satisfy corresponding universal-approximation theorems. \square

This equivalence between reachability and controllability does not hold for any kind of dynamics. Here we distinguish between reachability, describing whether a control state can be reached from any initial state, and controllability, which implies that any initial state can be driven to a target state via a control.

S1.3 Spatially Dependent Target

Here we describe how the CT-LTI microscopic target states (see Fig. 4a) are created. The node target and initial state values are dependent on the node position in the graph. All nodes are initialized with a state value of 0. We then choose one or more nodes in the graph, which we term *central nodes*. These nodes are assigned a state value $x_j = p(x = \mu)$, where p is the probability density function of the normal distribution $N(\mu, \sigma)$. Every node in the graph updates its value based on the shortest-path length from any other central node according to

$$x_i = x_i + \sum_j p \left(\mu + \frac{\text{shortest_path_length}(i, j)}{c} 3\sigma \right) \quad (\text{S6})$$

where c is some constant to normalize the shortest-path length. The factor 3σ is used to scale the normalized shortest path output within 3 standard deviations from the mean value. For example, if we set $c = 10$, then all nodes that have shortest path length greater than 10 are assigned a value less than $p(\mu + 3\sigma)$, which is very close to 0. By using this assignment method each node is assigned a value, which is spatially dependent, i.e. their values are dependent to the distance from a fixed node in the graph.

S1.4 Neural Network Architecture Details

For non-linear dynamics, the NN architecture that we used for LTI systems often leads to ODE stiffness and other numerical instabilities, such as exploding losses and weights. This could potentially be a result of the large number of parameters, as small parameter changes may lead to highly non-linear controls that make the ODE stiffer. For that reason, we use a graph neural network (GNN) architecture, which reduces the parameters and also utilizes the knowledge of the graph structure. For non-linear control, feedback control yielded higher performance, as it can be efficiently combined with the GNN architecture. The convolutional layer takes a tensor $\tilde{\mathbf{z}}$ of shape $c_{\text{in}} \times N \times \max_degree(G)$ as input, where c_{in} is the number of input channels. Each input channel is assigned to the respective states of SIR-X (ι, s, r, q), yielding $c_{\text{in}} = 4$ channels. N tensors out of c_{in} channels are stacked together, with each tensor representing the input of each node in the graph. The maximum degree of the network is used to determine the input vector for each node and a given channel. The node input contains only the state values of its direct neighbors $\mathcal{A}_{i,j} = 1$ and is padded with 0s to match the maximum degree. Graph neural network models are more stable and the use of ReLU activation is again possible. ReLUConvolutional layers are stacked ξ times, until the last dimension of the input tensor reaches the minimum value closer to 2. Each convolutional layer has a different number of output channels, and its filters slide across the last dimension of its input with a kernel shape 3×1 and stride 1. We connect the convolutional layers with average pooling layers that have kernels of size 2×1 producing an output with the same dimensions as the network input before channel assignment of states. The output can then be given to the network as input. This process input-output-input process is repeated several times, by setting the output of the average pooling as input and re-feeding it to the convolutions. This is referred to as message-passing or information propagation and is done

to ensure that nodal information is passed to non-direct neighbors via the hidden-state outputs that are reused as inputs. Four message passes are used in our experiments, and the rest of the layers are relevant to the control structure (e.g., number of elements) and constraints. When message passing terminates, the output dimensions are reduced as its channels are averaged to a vector of size N . The vector inner product of the averaged hidden state the driver matrix is calculated, thus allowing only relevant values to the control nodes to be used for control. A softmax layer is then applied, converting the values of all control nodes to a probability of assigning budget to that node. All node values can be considered the logits of that softmax operation. As non-driver nodes values are also fed to the softmax with value of zero, the neural network learns to push the softmax values of this nodes to zero. Each driver node is assigned budget proportional to its assigned probability. All non-driver node probabilities are masked to zero to disallow leaks of budget outside of driver nodes. This mechanism follows the intuition behind attention mechanisms [17], shifting control attention to the driver nodes that the model determines as more crucial. In the described case, we train NNC for 100 epochs.

S1.5 Other Graph structures

The results observed for the lattice are also confirmed for Barabási–Albert and random tree graphs. As summarized in tables S1 to S4, NNC preserves the low-loss/low-energy behavior for different graph structures. Furthermore, average control correlations over all samples in the macroscopic case are even higher for these graphs. SIRX dynamics are only tested on the lattice graph for the sake of visual clarity and interpretability of baselines controls. While running our experiments, other graph structures were successfully tested, but a rigorous research on non-linear dynamics and different graph structures will be conducted in the future.

S1.6 MSE loss and induced gradient

Our results indicate that NNC control signals $\mathbf{u}(t; \mathbf{w})$ (see Algorithm 1) are strongly correlated with optimal control signals that minimize the energy

$$\mathcal{E}[\mathbf{u}(t)] = \int_0^T \|\mathbf{u}(t)\|_2^2 dt. \quad (\text{S7})$$

The NNC algorithm (see Algorithm 1) is based on minimizing the mean square loss

$$J(t) = \frac{1}{N} \|\mathbf{x}^* - \mathbf{x}(t)\|_2^2 \quad (\text{S8})$$

in terms of a gradient descent

$$\mathbf{w}(n+1) = \mathbf{w}(n) - \eta \nabla_{\mathbf{w}(n)} J(T; \mathbf{w}(n)), \quad (\text{S9})$$

where η is the learning rate. Note that $\mathbf{x}(t)$ in Eq. (S8) is a function of $\mathbf{u}(t; \mathbf{w})$.

We can expand $\mathbf{u}(t; \mathbf{w}(n+1)) = \mathbf{u}(t; \mathbf{w}(n) + \Delta \mathbf{w}(n))$ with $\Delta \mathbf{w}(n) = -\eta \nabla_{\mathbf{w}(n)} J(T; \mathbf{w}(n))$ for small $\Delta \mathbf{w}(n)$ and fixed t :

$$\mathbf{u}(t; \mathbf{w}(n+1)) = \mathbf{u}(t; \mathbf{w}(n)) + \mathcal{J}_{\mathbf{u}} \Delta \mathbf{w}(n), \quad (\text{S10})$$

where $\mathcal{J}_{\mathbf{u}}$ is the Jacobian of \mathbf{u} with elements $(\mathcal{J}_{\mathbf{u}})_{ij} = \partial \mathbf{u}_i / \partial \mathbf{w}_j$. Note that $\Delta \mathbf{w}(n)$ can be made arbitrarily small using a small learning rate.

Since $\Delta \mathbf{w}(n) \propto \nabla_{\mathbf{w}(n)} J(t; \mathbf{w}(n))$ and

$$\nabla_{\mathbf{w}(n)} J(t; \mathbf{w}(n)) = \mathcal{J}_{\mathbf{u}}^T \nabla_{\mathbf{u}} J, \quad (\text{S11})$$

we find

$$\mathbf{u}(t; \mathbf{w}(n+1)) = \mathbf{u}(t; \mathbf{w}(n)) - \eta \mathcal{J}_{\mathbf{u}} \mathcal{J}_{\mathbf{u}}^T \nabla_{\mathbf{u}} J. \quad (\text{S12})$$

Based on the outlined arguments, we conclude that a gradient descent in \mathbf{w} may induce a gradient descent in \mathbf{u} according to Eq. (S12), where the square matrix $\mathcal{J}_{\mathbf{u}} \mathcal{J}_{\mathbf{u}}^T$ acts as linear transformation on $\nabla_{\mathbf{u}} J$.

In Fig. S2a, we show a typical evolution of $\|\mathbf{u}\|_2$ and $\|\mathbf{w}\|_2$ over 2000 training epochs and observe that $\|\mathbf{u}\|_2$ indeed evolves in a qualitatively similar manner as $\|\mathbf{w}\|_2$, as expected from Eqs. (S9) and (S12). As the norm $\|\mathbf{u}\|_2$ of the learned control input approaches the optimal control norm value

(green dashed line in Fig. S2a), the corresponding MSE reaches a minimum (see Fig. S2b). Another clear indicator for the described induced gradient descent are the positive correlations between $\|\mathbf{u}(n) - \mathbf{u}(n-1)\|_2$ and $\|\mathbf{w}(n) - \mathbf{w}(n-1)\|_2$ that we show in Fig. S2c.

It is also important to note that the current neural network parameter initialization produces very low energy control trajectories before training, due to the way how neural networks are initialized. We provide a statistical argument for this, by finding the empirical distribution of energy control $\mathcal{E}[\mathbf{u}(t; \mathbf{w}(0))]$ (see Fig. S8). In that case, the initial control trajectories in the provided NNC ELU FC architecture start with energy values way lower than optimal control, distributed in the interval $[5, 7]$. During training, gradient descent induced in \mathbf{u} slowly increases the energy of the control until it finds one that minimizes loss. The previous observations of induced gradient descent together with the NNC initialization (low energy distribution) provide empirical arguments for the implicit energy regularization of NNC.

S1.7 Nonlinear Network SIRX dynamics

The budget constraint (see Sec. 4.2) and the ability to only control driver nodes do not allow to create dense impenetrable walls of containment, as an infection can still pass through contained nodes at a lower rate. As TCC is a static control it already protects the driver nodes from $t = 0$ on, so TCC-controlled nodes will be infected very slowly. Assigning all budget to all driver nodes of interest also minimizes wasted “containment” budget. Still, distributing the budget to a smaller number of nodes increases the L2 norm of the control, making controls very expensive when considering quadratic energy costs. To have a control with less energy, it is important to distribute the budget to more nodes, therefore enabling more global containment and less containment on the target sub-graph. In Fig. S3, we show that NNC actually uses the control to slowly drive the epidemic to places that it can better contain. Still, for RL and NNC, we see that after some time controls reemerge on areas that were initially infected. This could be a learning artifact or a control effort to minimize infection peaks caused from delayed infections. For our experiments we choose that infection rate $\beta = 6$, recovery rate $\gamma = 1.8$, and $R_0 = \beta/\gamma = 3.33$. For all controls the budget is 600. The loss that NNC minimizes is defined as:

$$J(w) = [\max_{t \leq T} \bar{I}_{G^*}(t)]^2. \quad (\text{S13})$$

Back-propagation happens at time $t^* = \arg \max_{t \leq T} J(w)$. This time is approximated by preserving a sample of states when using the ODEsolve, and picking the maximum observed peak infection from that sample.

S1.8 Reinforcement Learning Baselines in SIRX

Reinforcement learning results are not included in the main paper, as our goal was to introduce a new specialized control framework. In this section, we compare our NNC results with those obtained using RL. Reinforcement learning is often described as “model-free” and addresses the (i) prediction problem and (ii) control problem [15]. We note that RL approaches may suffer from credit assignment challenges, where a reward signal is uninformative regarding the specific actions (especially in terms of time) that help reach the goal [14]. In contrast to RL, the proposed NNC is not model-free and the underlying gradient descent is directly calculated from the loss function. Therefore, we do not need to consider value prediction and credit assignment. It is possible to design a model-free NNC by learning the underlying system dynamics simultaneously with control, which could be an interesting future extension of our work. Note that a direct performance comparison between RL and NNC in terms of target loss may be considered unfair especially towards RL methods, unless extensive hyper-parameter optimization is performed beforehand.

We first implement SIRX dynamics as an RL environment. The softmax operation and budget assignment discussed in Sec. S1.4 take place in the environment and RL computes the softmax logit values over all driver nodes. Reinforcement learning is allowed to interact with the environment in a fixed interaction interval $\Delta t = 10^{-2}$. A2C and SAC implementations are taken from Stable-Baselines¹. Both implementations were tested for different parameter sets and trained for at least 50000 steps/epochs. Unfortunately, no implementation was able to “flatten the curve” considerably better than random control. Next, we use the TD3 implementation from Tianshu², which currently

¹ <https://github.com/DLR-RM/stable-baselines3>

² <https://github.com/thu-ml/tianshou>

showcases high-speed benchmarks and allows more customization of policy/critic architectures. The corresponding RL training takes around 17 seconds per epoch, whereas NNC takes approximately 5.5 seconds per epoch. Neither TD3 or NNC fully utilized the GPU in terms of computing and memory resources, often staying below 50% of usage, while memory utilization usually was below 10GB per method.

We show an overview of the hyperparameters that we use to train TD3 in Table S6. For more detailed explanations of these hyperparameters, see Ref. [4] and the Tianshu documentation³. Several baseline architectures in RL frameworks are often fully-connected multilayer perceptrons. Still, we observe that the graph neural network presented in Fig. 3b was more efficient in converging rewards in less computation time. We trained all models for 100 epochs and stored and evaluated the best model. In SAC and A2C, one training environment was used, whereas TD3 was sampling from two independent environments simultaneously due to its computational speed.

In terms of parameters both the TD3 policy network and NNC GNN have exactly the same parameters, but training is very different, as the gradient flows presented in Algorithms 1 and 2 and Fig. 2 cannot happen. The value function is now used for the calculation of similar gradients by predicting the cumulative reward signal. We studied several possible reward designs, and in the end we rigorously tested the following rewards:

The first reward signal we tested is calculated based on the mean number of infected nodes belonging to the target sub-graph $\bar{I}_{G^*}(t)$ at time t :

$$r_1(t) = -(\bar{I}_{G^*}(t))^2 \Delta t. \quad (\text{S14})$$

Although this reward seemingly provides direct feedback for an action, it also leads to several challenges. First, it does not necessarily flatten the curve, but it minimizes the overall infection through time. Such a reward could, for instance, potentially reinforce actions that lead to “steep” peaks instead of a flattened infection curve, as in practice it minimizes the area under the $I(t)$ curve. Furthermore, as current containment controls may have effect if applied consistently and in the long term, such reward design suffers from temporal credit assignment, since the reward value depends on a long and varying sequence of actions. Finally, any actions that happen after the peak infection occurrence will still be rewarded negatively, although such actions do not contribute to the goal minimization.

The next reward

$$r_2(t) = \begin{cases} 0 & , \text{if } t < T \\ -(\max_{t \leq T} \bar{I}_{G^*}(t))^2 & , \text{otherwise} \end{cases} \quad (\text{S15})$$

is designed to overcome the aforementioned shortcomings. This reward signal is sparse through time, as it is non-zero only at the last step of the control when the infection peak is known. The main property of interest of Eq. (S15) is that it has the same value as the loss that we used to train NNC (see Eq. (S13)). This reward signal also suffers from credit assignment problems. As the reward is assigned at a fixed time and not as a direct result of the actions that caused it, the corresponding reward dynamics is non-Markovian [16]. To address challenges caused by rewards with non-Markovian properties, reward shaping[3] and recurrent value estimators [10] can be used. Furthermore, n -step methods or eligibility traces can be evaluated if we expect the reward signal to be Markovian but with long and/or varying time dependencies.

The final reward $r_3(t)$ that we evaluated and used in the presented results is designed with two principles in mind:

$$\sum_t r_3(t) \propto \max_{t \leq T} (\bar{I}_{G^*}(t))^2 \quad (\text{S16a})$$

$$\arg \min_{t \leq T} \sum_t r_3(t) = \arg \max_{t \leq T} (\bar{I}_{G^*}(t)). \quad (\text{S16b})$$

Following those principles, the reward signal is approximately proportional to and provides information about the value of the infection peak used in the NNC loss calculation. The reward sum minimizes exactly at the time when peak infection occurs. This property is expected to reduce effects

³<https://tianshou.readthedocs.io/en/latest/api/tianshou.policy.html?highlight=td3#tianshou.policy.TD3Policy>

of temporal credit assignment. When aiming to replace the proportionality in Eq. (S16a) with an equality, we reach the following reward signal design:

$$r_3(t) = \begin{cases} 0 & , \text{ if } \bar{I}_{G^*}(t) \leq \max_{\tau < t}(\bar{I}_{G^*}(\tau)) \\ -\bar{I}_{G^*}^2(t) + (\max_{\tau < t} \bar{I}_{G^*}(\tau))^2 & , \text{ otherwise} \end{cases} \quad (\text{S17})$$

It is straightforward to show that Eq. (S17) indeed satisfies $\sum_t r_3(t) = \max_{t \leq T}(\bar{I}_{G^*}(t))^2$ and Eq. (S16b). This reward greatly improved performance without resorting to recurrent value estimators or further reward shaping. Still, after all proposed reward design and hyper-parameter optimization, NNC still has a higher performance (see Fig. S6a), although TD3 performs better than random control.

In Fig. S3a and S3b the dynamic controls of both RL and NNC seem to focus on protecting the target sub-graph by containing the infection as it spreads. In contrast to targeted constant control, they succeed in doing so by protecting driver nodes outside the target sub-graph. When comparing the dynamic control patterns, the budget allocation of NNC seems to be much more concentrated on specific nodes, and it creates more often contiguous areas of containment.

In Fig. S5 and S6, we also show the evolution of $S(t)$, $R(t)$, and $X(t)$. We observe that TCC and NNC show clear signs of flattening the curve by preserving the highest susceptibility fraction and lowest recovery fraction at time T , which can be interpreted as less susceptible nodes becoming infected and needing to recover. The random method outperforms the other frameworks in terms of effective containment fractions, as random control assignments at each time step let the disease spread such that higher infection fractions $I(t)$ are reached in the target sub-graph and therefore drivers with high infection fractions are effectively contained when controlled. Although low energy effective containment might seem favorable at first sight, it is not optimal in terms of flattening the curve with restricted budget, as it allows high infection fractions to occur within an area of interest. Budget restrictions often do not allow to fully constrain the spread in all infected nodes.

In Fig. S4, we observe that although RL does not converge in terms of critic and actor loss, it still converges to a higher reward. This confirms that RL is capable of controlling continuous dynamics with arbitrary targets, but it requires significant parametrization and training effort to have good stable value estimates.

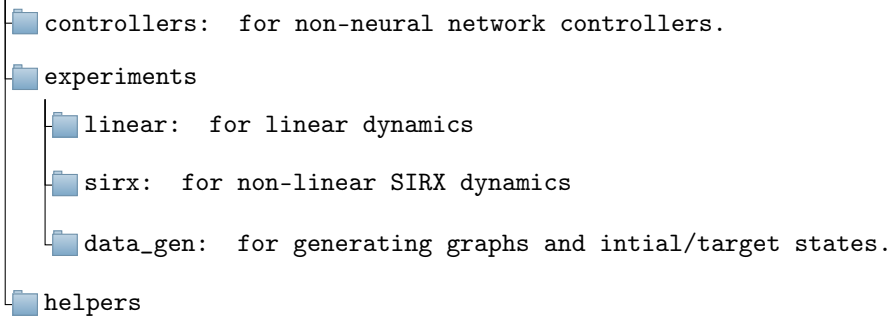
Finally, we tried to examine transfer learning capabilities from NNC to RL. A closer look at Fig. 3b and S7 reveals that the parametrized structures used for NNC and RL are the same, i.e. there are no weights in the control layers of Fig. 3b. This means that the architectures trained with NNC can be used as the “logit” action policy in RL, showcasing an effective use of transfer learning. In the given example, the RL policy network starting with trained NNC parameters, is further trained for 100 episodes. After training, RL had a similar performance as NNC since both methods flatten the curve at approximately $\bar{I}_{G^*} = 0.0788$. This means that RL did not improve the solution generated by NNC. This example can be used to illustrate the interplay between NNC and RL and how they can be used in synergy, e.g. when back-propagating through continuous dynamics is too expensive for high number of epochs. Reinforcement learning can be used as a meta-heuristic on top of NNC, and the latter can be treated as an alternative to imitation learning.

S1.9 Hardware and code

Our experiments were mainly conducted on a dedicated server that was equipped with an NVIDIA TITAN RTX GPU, 64GB of RAM, and an Intel I9 8-core 9900KF processor. Source files including a README and IPython scripts are provided in the attached supplemental material. Partial code tests with assertions were conducted to examine (i) stiffness, (ii) numerical errors or bugs, and (iii) validity and similarity of the same dynamics controlled by different models.

The code project general structure is organized as follows:

nnc-code



S1.10 Figures

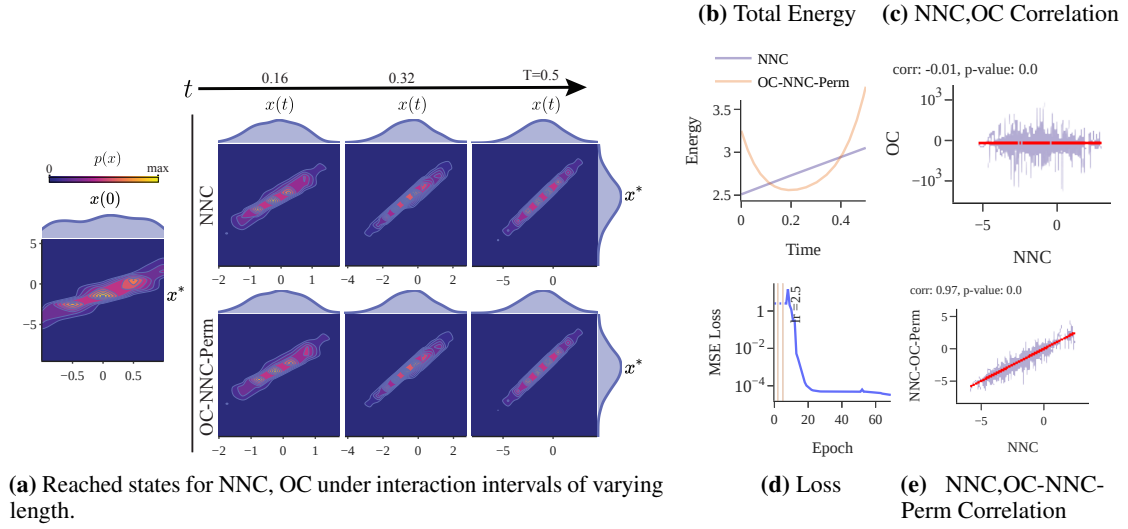


Figure S1: Comparison of NNC and OC controls on a single macroscopic control sample on a lattice. Results look similar for other samples.

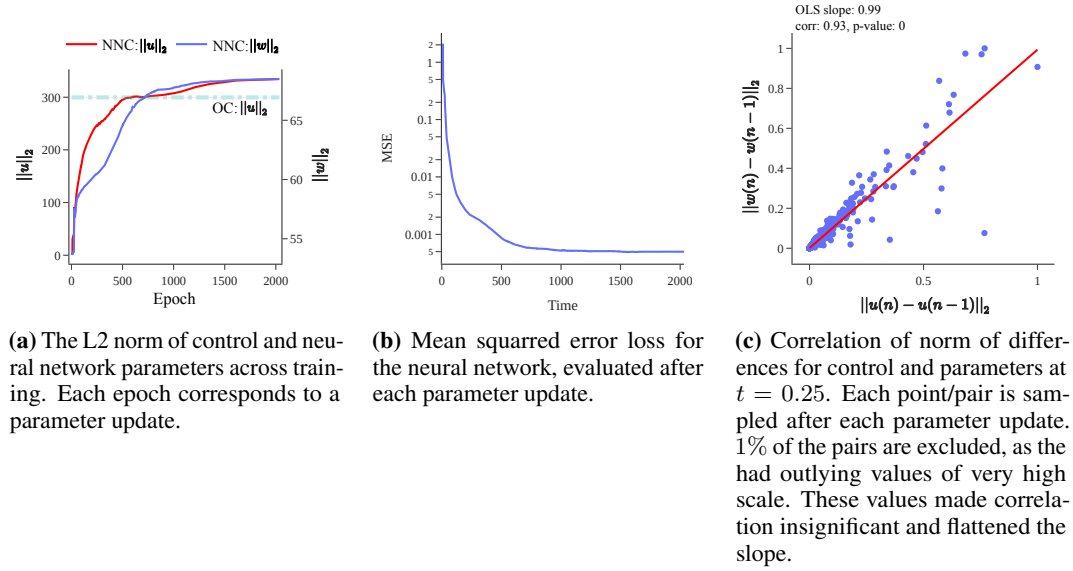
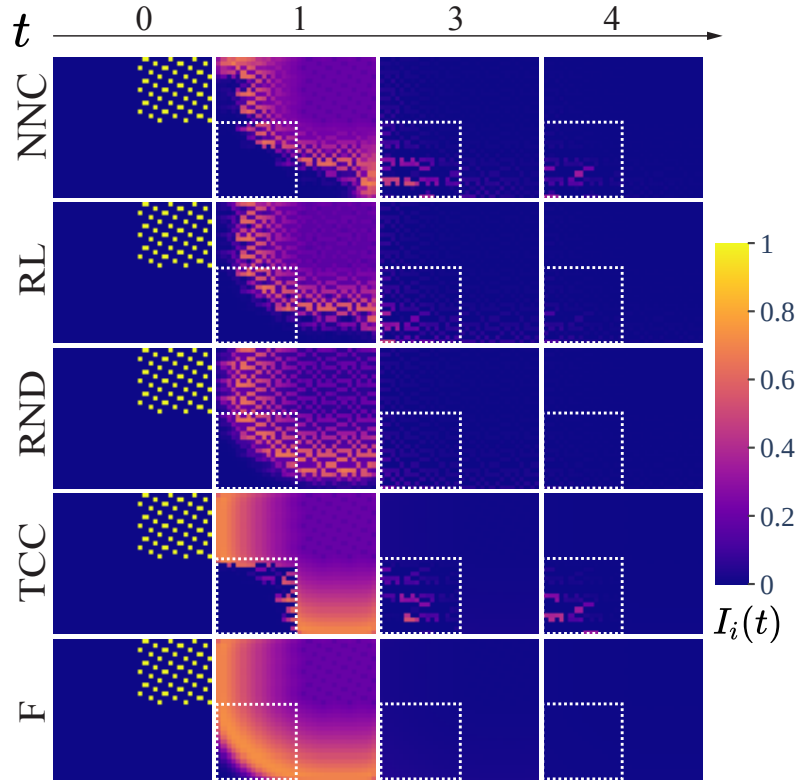
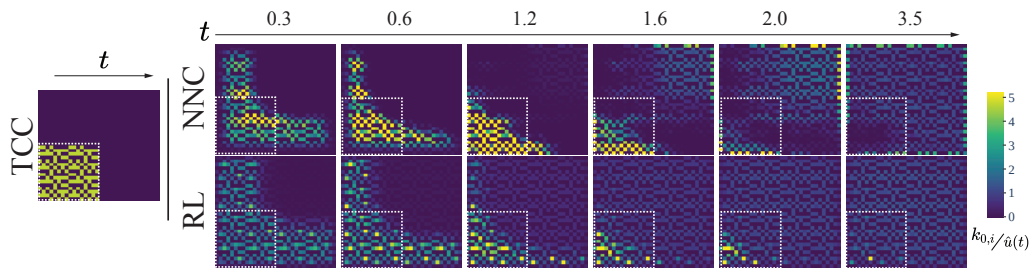


Figure S2: Energy, MSE, and L2 norm difference for consecutive NNC.

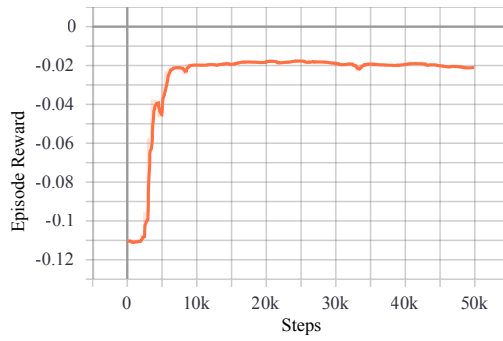


(a) Infection spread on lattice for all baselines.

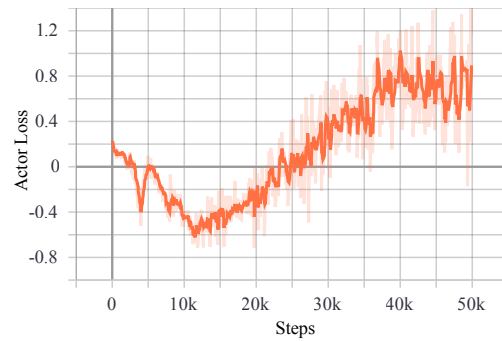


(b) Controls of RL, NNC and TCC.

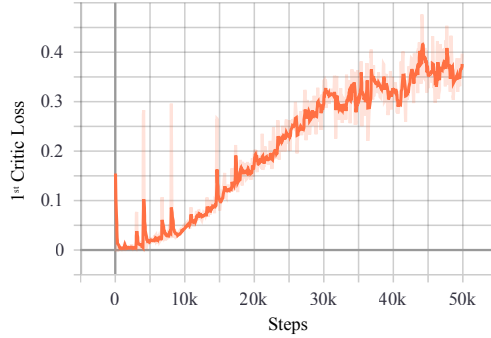
Figure S3: Infection spread and control from baselines. Target subgraph is approximately bounded by the white dotted lines.



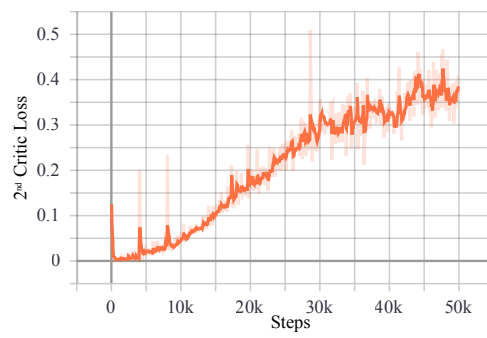
(a) Total episode reward as TD3 trains.



(b) Actor loss as TD3 trains.

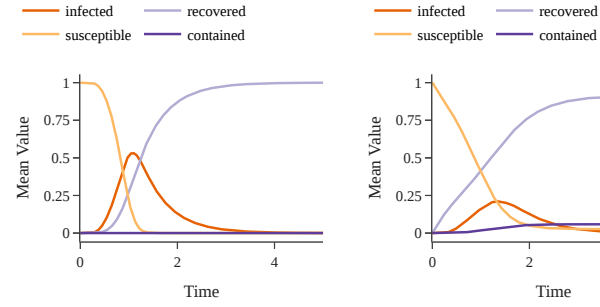


(c) First critic loss.

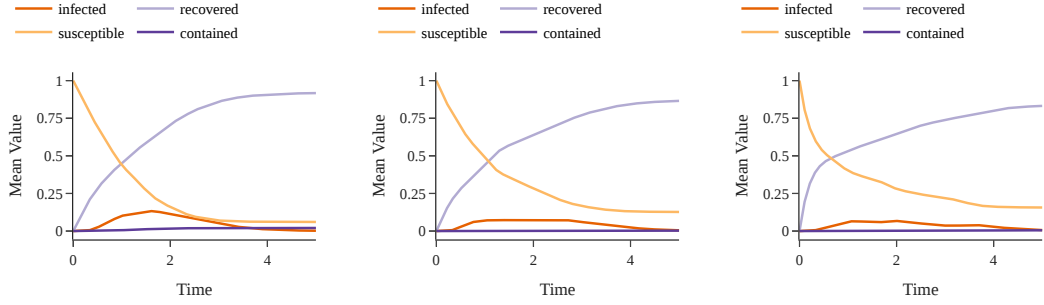


(d) Second critic loss.

Figure S4: RL learning performance evaluation plots using Tensorboard using 0.8 smoothing.



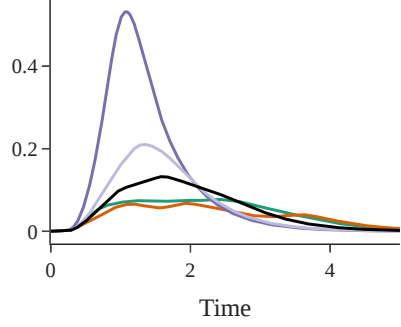
(a) SIRX curves for no control (F) baseline. (b) SIRX curves for random control (RND) baseline.



(c) SIRX curves for reinforcement learning control (RL) baseline. (d) SIRX curves for neural network control (NNC) baseline. (e) SIRX curves for targeted constant control (TCC) baseline.

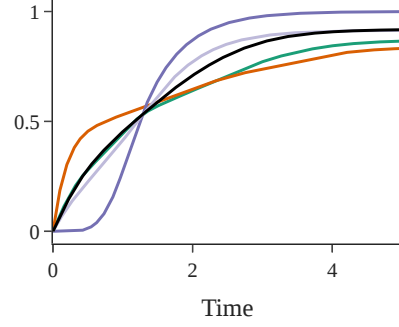
Figure S5: SIRX curves for all baselines in the target subgraph G^* .

— NNC — TCC — F — RND
— RL



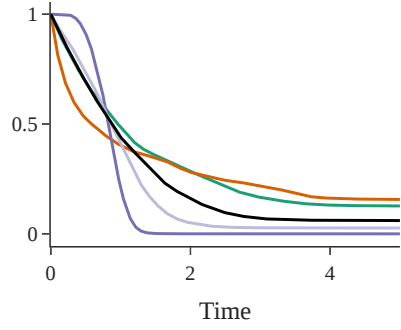
(a) Fraction of infected.

— NNC — TCC — F — RND
— RL



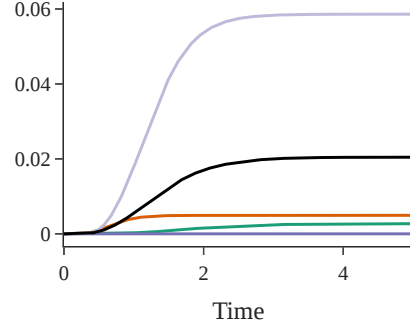
(b) Fraction of recovered individuals.

— NNC — TCC — F — RND
— RL



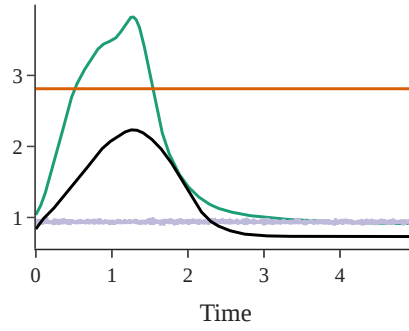
(c) Fraction of susceptible individuals.

— NNC — TCC — F — RND
— RL



(d) Effective containment fraction. It represents the value of infection negation by containment on drivers.

— NNC — TCC — RND
— RL



(e) Energy evolution for different control scenarios.

Figure S6: SIRX curves baseline comparisons for G^* .

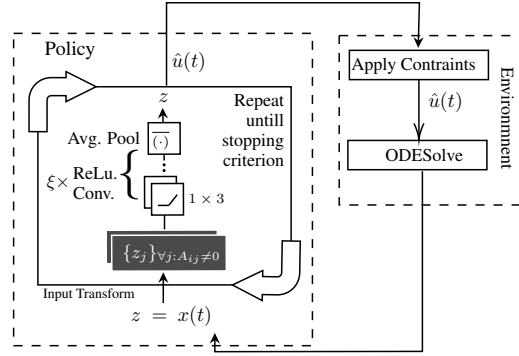


Figure S7: The change of control interactions when introducing RL. In contrast to the architecture discussed in Fig. 3b, all control constraints are applied outside the neural network.

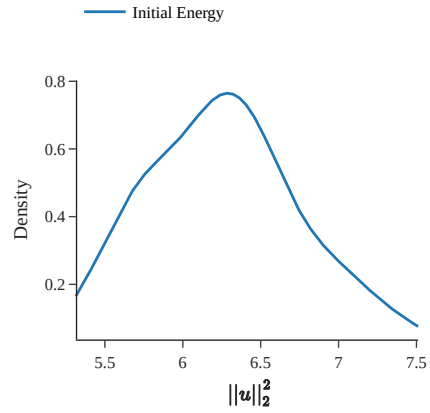


Figure S8: Distribution of initial L2 norm of control values for FC ELU NNC.

S1.11 Tables

Table S1: Microscopic results on Barabasi Albert graph.

Interval	Method	Energy		MSE loss		Wasserstein loss	
		Median	IQR	Median	IQR	Median	IQR
0.0001	NNC	1.87×10^4	3.13×10^3	3.4×10^{-6}	4.23×10^{-6}	2.94×10^{-6}	3.16×10^{-6}
	OC	1.68×10^4	3.9×10^3	7.16×10^{-7}	1.84×10^{-6}	6.04×10^{-7}	1.51×10^{-6}
0.001	NNC	1.88×10^4	3.13×10^3	3.18×10^{-4}	3.41×10^{-4}	1.79×10^{-4}	1.91×10^{-4}
	OC	1.68×10^4	3.91×10^3	1.44×10^{-5}	2.1×10^{-5}	1.27×10^{-5}	1.77×10^{-5}
0.01	NNC	1.84×10^4	2.79×10^3	1.84×10^{-2}	1.77×10^{-2}	8.49×10^{-3}	8.8×10^{-3}
	OC	1.71×10^4	3.97×10^3	1.07×10^{-3}	1.11×10^{-3}	6.76×10^{-4}	5.8×10^{-4}

Table S2: Miroscopic results on tree graph.

Interval	Method	Energy		MSE loss		Wasserstein loss	
		Median	IQR	Median	IQR	Median	IQR
0.0001	NNC	2.43×10^4	1.06×10^3	6.39×10^{-8}	4.16×10^{-8}	5.12×10^{-8}	2.51×10^{-8}
	OC	2.34×10^4	1.51×10^3	5.11×10^{-8}	4.62×10^{-9}	3.96×10^{-8}	1.9×10^{-9}
0.001	NNC	2.44×10^4	1.06×10^3	3.57×10^{-6}	4.13×10^{-7}	2.46×10^{-6}	2.33×10^{-7}
	OC	2.35×10^4	1.51×10^3	5.09×10^{-6}	4.27×10^{-7}	3.68×10^{-6}	6.06×10^{-7}
0.01	NNC	2.44×10^4	1.67×10^4	3.4×10^{-4}	8.93×10^{-2}	2.39×10^{-4}	6.18×10^{-2}
	OC	2.39×10^4	1.54×10^3	5×10^{-4}	4.33×10^{-5}	3.19×10^{-4}	1.09×10^{-4}

Table S3: Macroscopic results on Barabasi Albert graph.

Method	Energy		MSE		Wasserstein	
	Median	IQR	Median	IQR	Median	IQR
NNC	2.75×10^3	3.22×10^2	7.98	5.72×10^{-1}	2.42×10^{-4}	6.01×10^{-5}
OC	1.88×10^5	2.49×10^4	1.52×10^{-4}	9.43×10^{-5}	7.69×10^{-5}	2.29×10^{-5}
OC-NNC-Perm	2.72×10^3	3×10^2	2.43×10^{-4}	7.93×10^{-5}	2.06×10^{-4}	5.71×10^{-5}
OC-Perm	1.92×10^5	2.68×10^4	1.54×10^{-4}	1.12×10^{-4}	7.7×10^{-5}	3.13×10^{-5}

Table S4: Macroscopic results on tree graph.

Method	Energy		MSE		Wasserstein	
	Median	IQR	Median	IQR	Median	IQR
NNC	2.59×10^3	3.75×10^2	7.93	5.57×10^{-1}	1.4×10^{-4}	4.43×10^{-5}
OC	3.31×10^5	3.72×10^4	9.35×10^{-5}	1.21×10^{-5}	6.69×10^{-5}	6.43×10^{-6}
OC-NNC-Perm	2.58×10^3	3.76×10^2	9.2×10^{-5}	8.9×10^{-6}	8.98×10^{-5}	8.42×10^{-6}
OC-Perm	3.31×10^5	4.26×10^4	9.33×10^{-5}	1.25×10^{-5}	6.65×10^{-5}	7.84×10^{-6}

Table S5: Energy and peak infection evaluation including RL baseline.

Control	$\max_t(\bar{I}(t))$	$E(T)$
TCC	0.068	14059.7
NNC	0.078	8354.7
RL	0.132	5831.9
RND	0.210	4687.0
F	0.430	0.0

Table S6: TD3 parametrization

Hyper-Parameter	Value	Tested Values
Actor learning rate	0.0003	0.0003, 0.003, 0.03
Actor architecture	GNN	GNN, FC
Critics learning rate	0.0001	0.0001, 0.001, 0.01
Critics architecture	FC	FC
τ (Polyak update parameter)	0.005	0.005, 0.05
γ (discount factor)	0.99	0.5, 0.8, 0.99, 1
exploration noise	0.1	0.1
update frequency of actor parameters	4 epochs	1–4 epochs
policy noise	0.001	0.001, 0.01, 0.1
noise clip	0.5	0.5, 0.2
reward normalization	True	True, False

References

- [1] ANTSAKLIS, P. J., AND MICHEL, A. N. *A linear systems primer*. Springer Science & Business Media, 2007.
- [2] BROGAN, W. L. *Modern Control Theory (3rd Ed.)*. Prentice-Hall, Inc., USA, 1991.
- [3] CAMACHO, A., CHEN, O., SANNER, S., AND MCILRAITH, S. A. Non-markovian rewards expressed in ltl: guiding search via reward shaping. In *Tenth Annual Symposium on Combinatorial Search* (2017).
- [4] FUJIMOTO, S., HOOF, H., AND MEGER, D. Addressing function approximation error in actor-critic methods. In *International Conference on Machine Learning* (2018), pp. 1587–1596.
- [5] HANIN, B., AND SELLKE, M. Approximating continuous functions by relu nets of minimal width. *arXiv preprint arXiv:1710.11278* (2017).
- [6] KALMAN, R. E., ET AL. Contributions to the theory of optimal control. *Bol. soc. mat. mexicana* 5, 2 (1960), 102–119.
- [7] LESHNO, M., LIN, V. Y., PINKUS, A., AND SCHOCKEN, S. Multilayer feedforward networks with a nonpolynomial activation function can approximate any function. *Neural networks* 6, 6 (1993), 861–867.
- [8] LIU, Y.-Y., SLOTINE, J.-J., AND BARABÁSI, A.-L. Controllability of complex networks. *nature* 473, 7346 (2011), 167–173.
- [9] LYGEROS, J. On reachability and minimum cost optimal control. *Automatica* 40, 6 (2004), 917–927.
- [10] MIZUTANI, E., AND DREYFUS, S. E. Two stochastic dynamic programming problems by model-free actor-critic recurrent-network learning in non-markovian settings. In *2004 IEEE International Joint Conference on Neural Networks (IEEE Cat. No. 04CH37541)* (2004), vol. 2, IEEE, pp. 1079–1084.
- [11] SCHÄFER, A. M., AND ZIMMERMANN, H. G. Recurrent neural networks are universal approximators. In *International Conference on Artificial Neural Networks* (2006), Springer, pp. 632–640.
- [12] SONTAG, E. D., AND SIEGELMANN, H. On the computational power of neural nets. *J. Comp. Syst. Sci.* 50 (1995), 132–150.
- [13] STONE, M. H. The generalized weierstrass approximation theorem. *Mathematics Magazine* 21, 5 (1948), 237–254.
- [14] SUTTON, R. S. Temporal credit assignment in reinforcement learning. *PhD dissertation* (1985).
- [15] SUTTON, R. S., AND BARTO, A. G. *Reinforcement learning: An introduction*. MIT press, 2018.
- [16] THIÉBAUX, S., GRETTON, C., SLANEY, J., PRICE, D., AND KABANZA, F. Decision-theoretic planning with non-markovian rewards. *Journal of Artificial Intelligence Research* 25 (2006), 17–74.
- [17] VASWANI, A., SHAZEER, N., PARMAR, N., USZKOREIT, J., JONES, L., GOMEZ, A. N., KAISER, Ł., AND POLOSUKHIN, I. Attention is all you need. In *Advances in neural information processing systems* (2017), pp. 5998–6008.
- [18] YAN, G., REN, J., LAI, Y.-C., LAI, C.-H., AND LI, B. Controlling complex networks: How much energy is needed? *Physical review letters* 108, 21 (2012), 218703.
- [19] ZHOU, D.-X. Universality of deep convolutional neural networks. *Applied and computational harmonic analysis* 48, 2 (2020), 787–794.